IEEE Access
Multidisciplinary | Rapid Review | Open Access Journal

Received 8 June 2022, accepted 22 June 2022, date of publication 29 June 2022, date of current version 7 July 2022.

Digital Object Identifier 10.1109/ACCESS.2022.3186981

RESEARCH ARTICLE

Direct Yaw-Moment Control Integrated With Wheel Slip Regulation for Heavy Commercial Road Vehicles

HARSHAL PATIL[1], K. B. DEVIKA[1], (Member, IEEE), GUNASEKARAN VIVEKANANDAN[2], SRIRAM SIVARAM[2], AND SHANKAR C. SUBRAMANIAN[1], (Senior Member, IEEE)

[1]Department of Engineering Design, Indian Institute of Technology (IIT) Madras, Chennai 600036, India
[2]Madras Engineering Industries Private Ltd., Chennai 600058, India

Corresponding author: Shankar C. Subramanian (shankarram@iitm.ac.in)

This work was supported by the Ministry of Skill Development and Entrepreneurship, Government of India, under Grant EDD/14-15/023/MOLE/NILE. The work of Harshal Patil, K. B. Devika, and Shankar C. Subramanian was supported by Madras Engineering Industries Private Ltd. under Project RB1920ED660MADA008265.

ABSTRACT When a road vehicle is subjected to combined cornering and emergency braking, it potentially has a greater risk of wheel lock followed by loss of steerability and/or undesired yaw motion. While an Anti-lock Braking System (ABS) is mandatory in many countries to avoid wheel lock, more attention is required to its combined cornering and braking performance. This paper aims to design a Direct Yaw-Moment Controller (DYC) integrated with ABS to achieve vehicle directional stability for Heavy Commercial Road Vehicles (HCRVs). This study implements a robust reaching law-based sliding mode controller for DYC and ABS. The developed algorithm was evaluated in a Hardware-in-Loop (HiL) setup. The experimental results are compared for the integrated algorithm and standalone ABS algorithms. The proposed algorithm improved the Directional Performance Index (DPI) in the range of 29% to 84% over the open-loop behavior while maintaining vehicle stability. Moreover, it also improved the DPI in the range of 5% to 53% over standalone ABS in various emergency test cases.

INDEX TERMS Anti-lock braking system, differential braking, direct yaw-moment control, electronic stability control, pneumatic brakes, sliding mode control.

I. INTRODUCTION

Road traffic accidents are a global concern, with approximately 1.35 million human fatalities due to road vehicle crashes every year. The World Health Organization predicts traffic accident-related deaths will rise to the fifth position in the leading causes of human death by the year 2030 [1]. In the year 2019, India reported an average of 414 human fatalities every day due to road accidents. In the same year, accidents involving Heavy Commercial Road Vehicles (HCRVs) contributed to 31% of 151,113 total fatalities, despite their low share of total registered vehicles [2].

Accidents involving HCRVs often have severe repercussions such as loss of human lives and substantial financial loss. Development of Active Vehicle Safety Systems (AVSS) like Electronic Stability Control (ESC) and Anti-lock Braking System (ABS) is currently prioritized for improving road traffic safety. A study by the National Highway Traffic Safety Administration, USA, has concluded that the inclusion of ESC can help mitigate 14% loss of directional control crashes [3]. For the Indian road-traffic scenario, which varies from that of countries like the USA in terms of vehicle population and composition, operating practices, and road conditions, ESC in HCRVs is undoubtedly a way forward to help reduce accidents. From the year 2015, Indian legislation has made ABS mandatory for all classes of HCRVs having a gross vehicle weight of more than 12,000 kg [4]. Subsequently, ESC systems may become mandatory for a broader class of HCRVs in India over the next few years.

The associate editor coordinating the review of this manuscript and approving it for publication was Yiqi Liu.

A. ELECTRONIC STABILITY CONTROL IN THE LITERATURE

While ABS prohibits wheels from locking during braking, the ESC system controls the vehicle in an emergency to prevent directional instability. Directional instability may arise during an obstacle avoidance maneuver or a combined cornering and braking maneuver, especially on low friction surfaces. Various studies have investigated an obstacle avoidance scenario wherein the ESC intervenes by braking on one or more wheels to prohibit the vehicle from spinning and ensures lateral stability without a significant reduction in longitudinal vehicle speed [5]–[7]. However, a more complex case arises in combined cornering and emergency braking. When wheels are controlled to obtain maximum longitudinal forces, there is a significant reduction in lateral forces. The reason is the inherent coupling in lateral and longitudinal force generation. Thus, the objective of ESC in such a scenario is to ensure directional stability at the minimal expense of longitudinal performance. Several studies in the literature proposed integrating Direct Yaw-Moment Control (DYC), which involves an external yaw moment through differential braking to coordinate with ABS for directional stability. Although researchers have examined lateral stability with an integrated DYC and ABS to evaluate performance on split-friction roads [8], [9], only a few studies focused on combined cornering and braking maneuvers.

Table 1 shows a review of relevant studies on combined cornering and braking [10]–[14]. Overall the researchers utilized steady-state values of a dynamic lateral model for model reference control. Reference states represented nominal motion for given inputs, and tracking these variables in severe conditions ensured directional stability. The selection of tracking variables was the subject of investigation for the vehicle in the study to achieve lateral performance.

In the case of ABS, the task was to regulate wheel slip at the desired value to maximize braking performance. Sliding Mode Control (SMC) has been widely used to regulate wheel slip. Similarly, for DYC, researchers employed SMC [10], [14] or PID controllers [11], [13] for generating the desired yaw-moment profile. The advantage of using SMC is its robustness property, and it is highly favored in the control of nonlinear systems. However, it is confronted with chattering resulting in discontinuous control input activity. A reaching law-based SMC design serves to address the chattering issue. It involves defining a sliding surface and a reaching law to ensure that the state trajectory reaches the surface. Once reached, the state trajectory is insensitive to parametric uncertainty and external disturbances, thus ensuring robustness during the sliding motion towards the desired state [15]. However, an appropriate choice of reaching law becomes highly vital for a chatter-free operation. Researchers have collectively proposed constant rate, power rate, constant plus power rate reaching laws, and boundary layer methods for ABS or DYC. However, as shown by Devika and Thomas [16], the strategies mentioned above compromise robustness for chatter-free operation. Hence, the Power Rate Exponential Reaching Law (PRERL) presented in [16] that alleviates chattering while retaining robustness was used in the current study.

In an approach that considers directional stability in ABS design, Morrison and Cebon [12] developed a modified slip control strategy for examining the combined braking and cornering of articulated heavy vehicles. However, it required the driver's active intervention to maintain directional stability. In limits of tire-road traction, the driver may react in a wrong way; thus, the design of AVSS should consider minimizing the need for the driver to operate thoughtfully [17]. Thus, lateral performance without driver interference would give confidence in the AVSS algorithm's use in severe maneuvers.

In summary, there have been minimal studies in ABS evaluation for combined cornering and braking. Additionally, the literature on the development of DYC and ABS for the HCRV segment considering its challenges is limited.

B. CHALLENGES IN HCRVs

Compared with passenger cars, the design of AVSS is accompanied by additional challenges in the case of HCRVs. A significant load variation (typically a loading of 200% of the unladen weight) affects the vertical and longitudinal position of the center of gravity (CoG). Also, the larger CoG height and the suspension system have a prominent effect on the coupling of vehicle lateral and roll dynamics. Compared to the hydraulic brake system, air brakes in HCRVs have a larger response time ($\approx$ 0.6 s to reach 90% of the maximum pressure) [18]. HCRV tires are designed to reduce rolling resistance and tread wear, resulting in a lower peak friction coefficient, especially on wet road surfaces [19]. The characteristics mentioned above constitute the critical factors to be included in the design of AVSS, and the current study considers these in the proposed algorithm.

C. OBJECTIVE AND SCOPE

Based on the literature review and identified challenges, the following gaps in research on integrated DYC and ABS for HCRVs were identified. Only a few studies explored DYC integration with an ABS for a pneumatic brake actuator. Considering the slow response of pneumatic brake systems in HCRVs, it is essential to consider the actuator characteristics and then analyze the performance of DYC and ABS. In this regard, the literature is lean on performance evaluation using Hardware-in-Loop (HiL) or vehicle level testing. From a controller implementation perspective, most studies utilized the conventional reaching law-based SMC (such as constant rate reaching law, power rate reaching law, etc.). These controllers have limitations such as reduced robustness, slow-reaching speed, and chattering effects. Additionally, researchers have not analyzed the ABS design for cornering maneuvers and their effect on directional stability. This study attempts to address these gaps in the literature by examining the integrated DYC and ABS approach for the directional stability of an HCRV and provides an elaborate framework for its model-based design. The DYC incorporates a lateral dynamics model, including the influence of vehicle roll. A modified

TABLE 1. Literature survey on combined cornering and emergency braking.

S.R. No.	Author(s)	Tracking/ Regulation[1]	Control Method[2] ABS	Control Method[2] DYC	Reference Model (DYC)[3]	Vehicle Type[4]	Tire Model	HiL/VT Evaluation[5]	Test Cases
1	Bang et al. (2001) [10]	$\dot{\psi}$,λ	SMC	PID	SS, 2-DoF bicycle model	PC	Pacejka tire model	No	4
2	Yi et al. (2003) [11]	$\dot{\psi}$, β,λ	SMC	SMC	SS, 2-DoF bicycle model	PC	Pacejka tire model	No	1
3	Morrison and Cebon (2017) [12]	$\dot{\psi}$, β,ψ_{12},λ	SMC	RBA	SS, lateral dynamics model with roll coupling	HCRV	Fancher tire model	No	2
4	Wang et al. (2018) [13]	$\dot{\psi}$, β,λ	SMC	SMC	SS, 2-DoF bicycle model	PC	Magic Formula	Yes	2
5	Li et al. (2019) [14]	$\dot{\psi}$, β,λ	SMC	PID	2-DoF model for three-axle vehicle	HCRV	Dugoff tire model	Yes	5
6	**Current Study**	$\dot{\psi}$,λ	**SMC**	**SMC**	**SS, 3-DoF lateral dynamics model including roll coupling**	**HCRV**	**Magic Formula 6.1**	**Yes**	**4**

N/A: Not applicable, N/S: Not specified
[1]($\dot{\psi}$: Vehicle yaw rate, β: Vehicle sideslip angle, ψ_{12}: Articulation angle, λ: Wheel slip)
[2](SMC: Sliding Mode Control, RBA: Rule Based Algorithm)
[3](SS: Steady-state, DoF: Degrees of Freedom)
[4](PC: Passenger Car, HCRV: Heavy Commercial Road Vehicle)
[5](HiL: Hardware-in-Loop, VT: Vehicle-Testing)

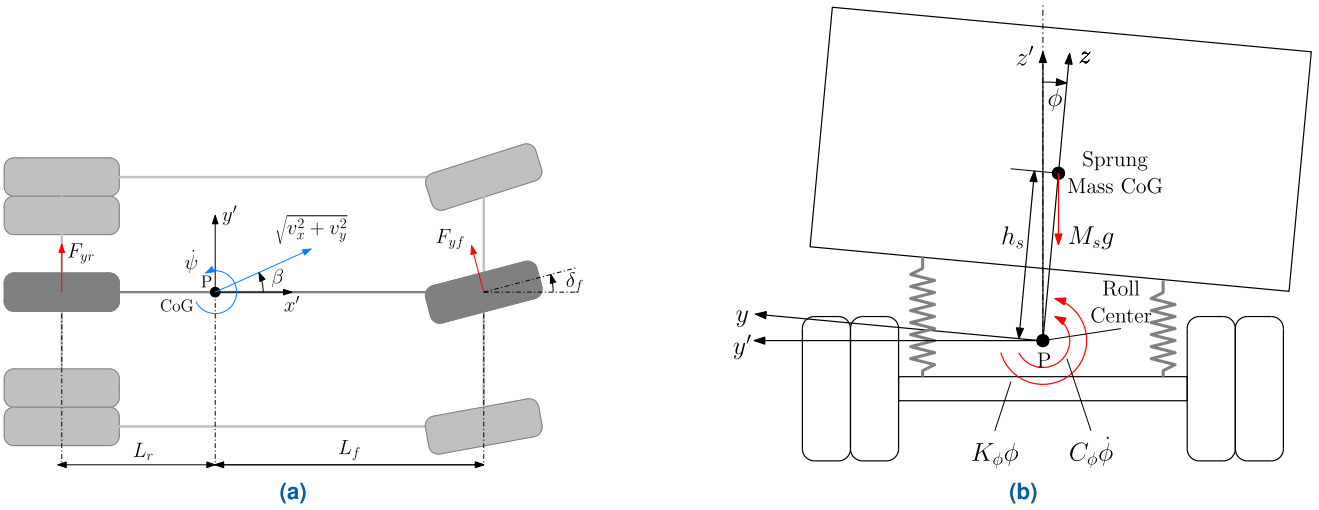

FIGURE 1. Free body diagram of a vehicle: (a) Yaw-plane motion; (b) roll motion of sprung mass.

model-based Wheel Slip Regulation (WSR) algorithm is presented as ABS considering longitudinal and lateral load transfer. Recognizing the inevitable modeling and parameter uncertainties, the framework effectively demonstrates the application of a robust reaching law-based sliding mode controller for this application. The necessary elements like delay compensation with a brake controller are incorporated to overcome the shortcomings of the actuator.

The scope of research is to employ the pneumatic brake actuator to control the longitudinal forces for obtaining directional stability and improving the lateral performance of an HCRV. Furthermore, this study explicitly analyses the combined cornering and braking scenario, evaluates the algorithm through HiL experiments, and compares its performance with the standalone ABS algorithm.

The organization of the paper is as the following. Section II describes the mathematical models derived for the design of direct yaw-moment control, wheel slip regulation, and brake controller. In Section III, the control design and brake force allocation strategy have been elaborated. HiL results are presented and discussed in Section IV, followed by conclusions in Section V.

II. SYSTEM MODELING

A. NONLINEAR LATERAL DYNAMICS MODEL INCLUDING ROLL

A nonlinear 8-DoF vehicle model derived for controller design is described in this section. Four of the eight degrees of freedom represent translations along the longitudinal and lateral axes and rotational displacements about the yaw and roll axes. The remaining four represent the rotational displacement of the individual wheel about its axis.

Fig. 1 depicts a free body diagram of the vehicle in its equivalent configuration for the case of yaw and roll motion while cornering. In the figure, g is the acceleration due to gravity, M_s is vehicle sprung mass, L_f and L_r respectively are distances of front and rear axle from vehicle center of gravity, h_s is the perpendicular distance of the sprung mass center of

gravity to roll axis, K_ϕ is suspension roll stiffness coefficient, C_ϕ is suspension roll damping coefficient, $\dot{\psi}$ is vehicle yaw rate, β is vehicle sideslip angle, ϕ is vehicle roll angle, and F_y is lateral ground force. The following assumptions were made to derive the mathematical model:

- Sprung mass was assumed to roll about the longitudinal axis (x'-axis).
- Roll of unsprung mass was considered negligible.
- Sprung and unsprung masses were assumed to have yaw motion around the vertical axis passing through point P on the roll axis (z'-axis).
- The vehicle roll angle was assumed to be small.
- The front and rear wheels were represented by a single equivalent front and rear wheel, respectively.

With the above assumptions and appropriate small angle approximations, a set of equations representing the mathematical model for an HCRV in combined braking and lateral motion considering roll dynamics was derived as [20]:

$$\begin{aligned} &M\left(\dot{v}_x(t) - v_y(t)\dot{\psi}(t)\right) + M_s h_s \dot{\phi}(t)\dot{\psi}(t) \\ &= F_{b,fl}(t) \\ &\quad + F_{b,fr}(t) + F_{b,rl}(t) + F_{b,rr}(t), \end{aligned} \tag{1}$$

$$\begin{aligned} &M\left(\dot{v}_y(t) + v_x(t)\dot{\psi}(t)\right) - M_s h_s \ddot{\phi}(t) \\ &= 2C_{\alpha f}\left(\delta_f(t) \right. \\ &\quad \left. + \epsilon_f(t) - \frac{v_y(t)}{v_x(t)} - \frac{L_f}{v_x(t)}\dot{\psi}(t)\right) + 2C_{\alpha r}\left(\epsilon_r(t) \right. \\ &\quad \left. - \frac{v_y(t)}{v_x(t)} + \frac{L_r}{v_x(t)}\dot{\psi}(t)\right), \end{aligned} \tag{2}$$

$$\begin{aligned} &I_x\ddot{\phi}(t) + I_{xz}\ddot{\psi}(t) - M_s h_s\left(\dot{v}_y(t) + v_x(t)\dot{\psi}(t)\right) \\ &= \left(M_s g h_s - K_\phi\right)\phi(t) - C_\phi\dot{\phi}(t), \end{aligned} \tag{3}$$

$$\begin{aligned} &I_z\ddot{\psi}(t) + I_{zx}\ddot{\phi}(t) \\ &= 2C_{\alpha f}L_f\left(\delta_f(t) + \epsilon_f(t) - \frac{v_y(t)}{v_x(t)} \right. \\ &\quad \left. - \frac{L_f}{v_x(t)}\dot{\psi}(t)\right) - 2C_{\alpha r}L_r\left(\epsilon_r(t) - \frac{v_y(t)}{v_x(t)} + \frac{L_r}{v_x(t)}\dot{\psi}(t)\right), \end{aligned} \tag{4}$$

where t denotes time, M is total vehicle mass, I_x and I_z respectively are the moments of inertia of sprung mass about the x-axis and a vertical axis passing through the vehicle center of gravity, I_{xz}/I_{zx} is the product of inertia for x and z axes, v_x and v_y respectively are longitudinal and lateral vehicle speeds, $C_{\alpha f}$ and $C_{\alpha r}$ respectively are the single front and rear wheel cornering stiffness, δ_f is front-wheel steer angle, F_b is the braking force, and wheel identifiers fl, fr, rl, and rr respectively indicate the front left, front right, rear left, and rear right wheels. This model also considers the axle roll steer (ϵ_f and ϵ_r respectively for the front and rear axles), which is assumed proportional to the vehicle roll through a proportionality constant $C_{\epsilon f}$ and $C_{\epsilon r}$. In the presence of an external yaw-moment ($M_{z,\text{ext}}$), the above model is described

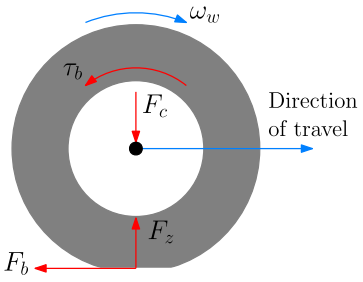

FIGURE 2. Free-body diagram of wheel in braking.

in the nonlinear state-space form,

$$\dot{\mathbf{x}}(t) = \mathbf{f}\left(\mathbf{x}(t), \delta_f(t), F_{b,ij}(t), M_{z,\text{ext}}(t)\right), \tag{5}$$

where $ij = \{fl, fr, rl, rr\}$, the state vector is,

$$\mathbf{x}(t) = \begin{bmatrix} v_x(t) & v_y(t) & \dot{\psi}(t) & \phi(t) & \dot{\phi}(t) \end{bmatrix}^\intercal, \tag{6}$$

δ_f, $F_{b,ij}$, $M_{z,\text{ext}}$ are the inputs, and $\mathbf{f}$ is a nonlinear function of states and inputs.

B. WHEEL SLIP DYNAMICS MODEL

The longitudinal force generated at the tire-road interface is a function of wheel slip ratio, λ, defined as,

$$\lambda(t) = \frac{v_{cx}(t) - R\omega_w(t)}{v_{cx}(t)}, \tag{7}$$

where R is the effective radius of the wheel, v_{cx} is wheel-center speed, and ω_w is wheel angular speed. The sign convention considered in this study is such that wheel slip is positive during braking. Also, the wheel lock condition during which the angular speed is zero corresponds to the value of λ being unity. The primary aim of ABS is to avoid wheel lock and regulate the wheel slip around its peak value to generate maximum braking force resulting in stable braking with lower braking distance (known as wheel slip regulation).[1]

Fig. 2 depicts the free-body diagram of a wheel being acted by braking torque. In the figure, F_c is wheel bearing force, F_z is vertical ground force, and τ_b is braking torque. Applying a moment balance equation along the wheel center gives,

$$\alpha_{w,ij}(t) = \frac{F_{b,ij}(t)R_{ij} - \tau_{b,ij}(t)}{I_{w,ij}}, \tag{8}$$

where I_w is wheel moment of inertia, and α_w is wheel angular acceleration. Also, the longitudinal component of the vehicle's velocity at CoG and wheel center-point velocity can be approximated to be equal in magnitude. Under this assumption, differentiating (7) gives the dynamics of wheel slip ratio as,

$$\dot{\lambda}_{ij}(t) = \frac{R_{ij}}{v_x(t)}\left(\frac{a_x(t)\omega_{w,ij}(t) - v_x(t)\alpha_{w,ij}(t)}{v_x(t)}\right), \tag{9}$$

[1] ABS will be referred to as WSR for the rest of the article.

where a_x is longitudinal acceleration. Upon substitution of the angular acceleration term from (8),

$$\dot{\lambda}_{ij}(t) = \frac{R_{ij}}{v_x(t)}\left(\frac{a_x(t)\omega_{w,ij}(t)}{v_x(t)} - \frac{\hat{F}_{b,ij}(t)R_{ij}}{I_{w,ij}}\right) + \frac{R_{ij}\tau_{b,ij}(t)}{v_x(t)I_{w,ij}}, \quad (10)$$

where $\hat{F}_{b,ij}$ is the estimated longitudinal force during braking. The longitudinal brake force can be expressed as,

$$\hat{F}_{b,ij}(t) = \hat{\mu}_x\Big(\lambda_{ij}(t), v_{cx,ij}(t), \alpha_{ij}(t)\Big)\hat{F}_{z,ij}(t), \quad (11)$$

where α is tire slip angle, and $\hat{\mu}_x$ is the estimated longitudinal coefficient of friction characterized by the tire model. Normal force at the tire-road interface ($\hat{F}_{z,ij}$) was calculated by decoupling the two axles and considering a virtual mass on each axle as derived in [21]. Thus, the expression for normal forces as a function of acceleration in the longitudinal and lateral direction is given by,

$$\begin{aligned}
\hat{F}_{z,fl}(t) &= M\left(\frac{L_r}{L}g - \frac{h}{L}a_x(t)\right)\left(\frac{1}{2} - \frac{ha_y(t)}{T_f g}\right),\\
\hat{F}_{z,fr}(t) &= M\left(\frac{L_r}{L}g - \frac{h}{L}a_x(t)\right)\left(\frac{1}{2} + \frac{ha_y(t)}{T_f g}\right),\\
\hat{F}_{z,rl}(t) &= M\left(\frac{L_f}{L}g + \frac{h}{L}a_x(t)\right)\left(\frac{1}{2} - \frac{ha_y(t)}{T_r g}\right),\\
\hat{F}_{z,rr}(t) &= M\left(\frac{L_f}{L}g + \frac{h}{L}a_x(t)\right)\left(\frac{1}{2} + \frac{ha_y(t)}{T_r g}\right), \quad (12)
\end{aligned}$$

where h is the distance of the center of gravity from the ground, T_f and T_r respectively are the front and rear track widths, and a_y is lateral acceleration. Thus, the wheel slip dynamics is represented as a nonlinear state-space model given by,

$$\dot{\lambda}_{ij}(t) = f_{ij}\Big(\lambda_{ij}(t), t\Big) + g_{ij}(t)\,\tau_{b,ij}(t), \quad (13)$$

where $\tau_{b,ij}$ is the input.

C. TIRE MODEL

This study employed the Magic Formula 6.1 truck tire model to calculate the longitudinal and lateral forces in combined slip. The general expression of the model is given by [22],

$$\begin{aligned}
y(x) &= D\sin\left[C\tan^{-1}\left\{Bx - E\big(Bx - \tan^{-1}(Bx)\big)\right\}\right],\\
Y(X) &= y(x) + S_v,\\
x &= X + S_h. \quad (14)
\end{aligned}$$

Here Y represents the output variable of interest (longitudinal or lateral force), and X represents the input variable (wheel slip or slip angle). The variables A, B, C, D, and E, represent stiffness, shape, peak, and curvature factors. The shift factors S_v and S_h represent respectively the vertical and horizontal shift of the curve. Parameters of the above model were experimentally determined and provided by IPG TruckMaker® for a 315/80R22.5 radial truck tire [23].

TABLE 2. Brake system parameters.

Parameter	Value	Unit
Gain, K_b	0.9	bar/V
Time constant, τ	260	ms
Time-delay, T_d	45	ms

D. BRAKE SYSTEM MODEL

The brake setup for the study uses an Electro-Pneumatic Regulator (EPR). It offers an advantage in terms of faster brake response compared to a conventional treadle valve in HCRVs. A first-order plus time delay model for the brake system was developed using linear time-invariant approximation by Sridhar et al. in [24], given by the transfer function (P),

$$P(s) = \frac{K_b}{1+\tau s}e^{-T_d s}, \quad (15)$$

where s is a complex variable. The brake system parameters were identified experimentally and are summarized in Table 2.

The state-space representation of the above input-delayed system can be expressed as,

$$\begin{aligned}
\dot{x}_b(t) &= A_b x_b(t) + B_b u(t - T_d),\\
P_{\text{act}}(t) &= C_b x_b(t), \quad (16)
\end{aligned}$$

where x_b is the state, u is the system input, P_{act} is the brake pressure output, and $\{A_b, B_b, C_b, 0\}$ is the state-space realization. The brake pressure was converted into brake torque utilizing a model for an S-cam type brake system as given in [18]. The model in a simplified form is given by,

$$\tau_b(t) = K_{\text{gain}}\left(P_{\text{act}}(t) - P_{\text{co}}\right), \quad (17)$$

where P_{co} is the contact pressure, and K_{gain} is the pressure to torque conversion gain. The model considered the efficiency of the brake system; however, the effects of temperature were neglected.

III. CONTROLLER DESIGN

Fig. 3 depicts a high-level functional block diagram of the 'integrated direct yaw-moment controller and wheel slip regulation' (DYC+WSR). The algorithm includes a reference model that specifies the ideal motion for the vehicle. Inputs to the model are the front steering wheel angle and vehicle's longitudinal speed, and output is the reference yaw rate. The DYC block compares the error in reference and actual yaw rate and outputs the required yaw moment. The WSR block computes the desired torque on each wheel by evaluating the error between the wheel slip's estimated and desired value. This study utilizes reaching law-based SMC in both the DYC and WSR algorithms.

The reaching law approach directly specifies the sliding function's dynamics. A desirable property in a reaching law-based SMC is the controller's fast response in the reaching phase and alleviated chattering. Moreover, for robustness, sliding mode motion should be ensured for a significant duration in the sliding phase. A Power Rate Exponential Reaching

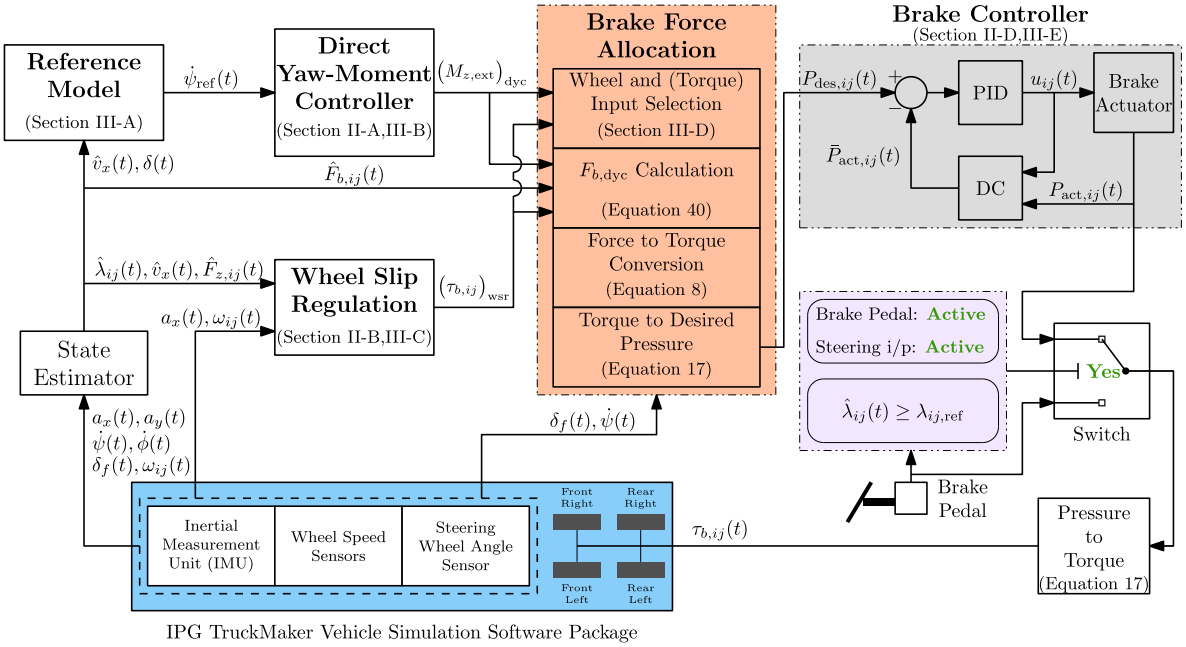

FIGURE 3. High-level functional block diagram of the integrated control algorithm.

Law (PRERL) having the traits above was proposed in [16] and is given as,

$$\dot{s}(t) = -\frac{K_0|s(t)|^{\beta_0}\mathrm{sgn}(s(t))}{\delta_0 + (1-\delta_0)e^{-\gamma_0|s(t)|^{\phi_0}}}, \tag{18}$$

where, s is the sliding function, K_0 is the SMC gain, and β_0 $(0 < \beta_0 < 0.5)$, δ_0 (< 1), γ_0 (> 0) and ϕ_0 (> 0) are other controller parameters. The power rate term $|s(t)|^{\beta_0}$ increases the reaching speed and has an advantage in chattering mitigation in the given range of β_0. The denominator of the reaching law guarantees significant sliding mode motion, thus ensuring robustness to external disturbances and parametric uncertainties. Subsequently, the brake force allocation strategy ensures that the desired moment is generated. Brake controllers on each wheel execute the final desired torque demand. Furthermore, most of the required vehicle states and the force/coefficient at the tire-road interface can be directly measured or estimated. For example, literature [25], [26] comprehensively reviews the different friction force/coefficient estimation methods. Vehicle state and parameter estimation has been demonstrated using the dual extended Kalman filters in studies [27], [28]. As the primary focus of this study was the performance evaluation and comparative analysis of the algorithm for a pneumatic brake actuator, this study assumes the availability of vehicle states and tire-road interface-related information. The experiments utilized this information from the vehicle dynamic simulation software IPG TruckMaker®.

A. REFERENCE MODEL

Vehicle instability in severe cornering maneuvers can be attributed to saturation of lateral forces as their relation is nonlinear to the increasing slip angle. Thus, as an ideal vehicle response, this study utilized a linear 3-DoF steady-state model to determine the reference yaw rate for tracking. For this purpose, the longitudinal speed was assumed to be constant, and model equations from Section II-A were rewritten to include the sideslip angle. Consequently, the state-space form is obtained as,

$$\mathbf{E}\dot{\mathbf{x}}(t) = \mathbf{A}\mathbf{x}(t) + \mathbf{b}\delta_f(t), \tag{19}$$

or

$$\dot{\mathbf{x}}(t) = \mathbf{E}^{-1}\mathbf{A}\mathbf{x}(t) + \mathbf{E}^{-1}\mathbf{b}\delta_f(t), \tag{20}$$

where the state vector

$$\mathbf{x}(t) = \begin{bmatrix}\beta(t) & \dot{\psi}(t) & \phi(t) & \dot{\phi}(t)\end{bmatrix}^{\mathsf{T}}, \tag{21}$$

and the input vector

$$\mathbf{b} = \begin{bmatrix}2C_{\alpha f} & 2C_{\alpha f}L_f & 0 & 0\end{bmatrix}^{\mathsf{T}}. \tag{22}$$

The matrices $\mathbf{E}$ and $\mathbf{A}$ are given as follows:

$$\mathbf{E} = \begin{bmatrix} Mv_x & 0 & 0 & -M_s h_s \\ 0 & I_z & 0 & I_{zx} \\ 0 & 0 & 1 & 0 \\ -M_s h_s v_x & I_{xz} & 0 & I_x \end{bmatrix}, \tag{23}$$

and

$$\mathbf{A} = \begin{bmatrix} \Theta_1 & \Theta_2 & \Theta_3 & 0 \\ \Theta_4 & \Theta_5 & \Theta_6 & 0 \\ 0 & 0 & 0 & 1 \\ 0 & M_s h_s v_x & M_s g h_s - K_\phi & -C_\phi \end{bmatrix}, \tag{24}$$

where Θ_1 to Θ_6 are defined in Appendix A. From the above model, steady-state values as a function of speed and front-wheel steer angle were obtained by setting the state

vector's time-derivative to zero. Then, the steady-state vector ($\mathbf{x}_{ss}$) is given by,

$$\mathbf{x}_{ss}(t) = -\mathbf{A}(v_x)^{-1}\mathbf{b}\delta_f(t). \tag{25}$$

Thus, the reference yaw rate ($\dot{\psi}_{ref}$) is given by,

$$\dot{\psi}_{ref}(t) = \begin{bmatrix} 0 \\ 1 \\ 0 \\ 0 \end{bmatrix} \cdot \mathbf{x}_{ss}(t). \tag{26}$$

B. DIRECT YAW-MOMENT CONTROL

A sliding mode controller based on the model described in Section II-A was employed for obtaining the yaw-moment. The tracking variable considered was the vehicle yaw rate. Hence, the sliding function (s_1) was defined as an error between the current and reference yaw rate, expressed as,

$$s_1(t) = \dot{\psi}(t) - \dot{\psi}_{ref}(t). \tag{27}$$

To apply the reaching law, the dynamics of sliding function was obtained as,

$$\dot{s}_1(t) = \ddot{\psi}(t) - \ddot{\psi}_{ref}(t). \tag{28}$$

From the model equations in Section II-A, an explicit relation can be derived for the time derivative of vehicle yaw rate in terms of vehicle parameters, states, and the external yaw-moment as,

$$\begin{aligned}\ddot{\psi}(t) = B_\beta v_y(t) + B_r\dot{\psi}(t) + B_\phi\phi(t) + B_p\dot{\phi}(t) \\ + B_\delta\delta_f(t) + B_\tau M_{z,ext}(t).\end{aligned} \tag{29}$$

The expressions for the coefficients (B_β, B_r, B_ϕ, B_p, B_δ, and B_τ) in the equations are given in the Appendix A. Substituting the expression for $\ddot{\psi}(t)$ from (29) into (28), and using PRERL, the control input $M_{z,ext}$ is obtained as,

$$\begin{aligned}\left(M_{z,ext}(t)\right)_{dyc} = -\frac{1}{B_\tau}\Bigg[&\frac{K_1|s_1(t)|^{\beta_1}\mathrm{sgn}(s_1(t))}{\delta_1 + (1-\delta_1)e^{-\gamma_1|s_1(t)|^{\phi_1}}} \\ &+ B_\beta v_y(t) + B_r\dot{\psi}(t) + B_\phi\phi(t) \\ &+ B_p\dot{\phi}(t) + B_\delta\delta_f(t) - \ddot{\psi}_{ref}(t)\Bigg],\end{aligned} \tag{30}$$

where K_1, β_1, δ_1, γ_1, and ϕ_1 are controller parameters, and subscript $(\cdot)_{dyc}$ indicates its affiliation to DYC. Subsequently, the task was to generate this moment by appropriately allocating the brake forces, as described in Section III-D.

In reality, a disparity always exists between the actual vehicle dynamics and the mathematical model due to the model parameter's uncertainty, unmodeled dynamics, and external disturbances. Accounting for these model inaccuracies, (29) can be expressed as,

$$\begin{aligned}\ddot{\psi}(t) = B_\beta v_y(t) + B_r\dot{\psi}(t) + B_\phi\phi(t) + B_p\dot{\phi}(t) \\ + B_\delta\delta_f(t) + B_\tau M_{z,ext}(t) + \tilde{f}\left(\mathbf{x}(t)\right),\end{aligned} \tag{31}$$

where $\mathbf{x}$ is the state vector as given in (6), and $\tilde{f}$ is an unknown bounded function that represents model uncertainties and disturbances. Here, the uncertainties and disturbances are assumed as additive perturbations to the system [29], [30]. Defining a Lyapunov function for the above system as,

$$V(t) = \frac{1}{2}s_1^2(t), \tag{32}$$

and differentiating with respect to time gives,

$$\dot{V}(t) = s_1(t)\dot{s}_1(t). \tag{33}$$

Substituting equations (30) and (31) in (33),

$$\dot{V}(t) = s_1(t)\tilde{f}\left(\mathbf{x}(t)\right) - K_1\rho_1|s_1(t)|, \tag{34}$$

where $\rho_1 > 0$ and is expressed as,

$$\rho_1 = \frac{|s_1(t)|^{\beta_1}}{\delta_1 + (1-\delta_1)e^{-\gamma_1|s_1(t)|^{\phi_1}}}. \tag{35}$$

Assuming that $|\tilde{f}| < \tilde{F}$ and letting $K_1 = \tilde{F} + \eta$ yields,

$$\dot{V}(t) < -\eta\rho_1|s_1(t)|. \tag{36}$$

Since $\dot{V} < 0$ for $s_1 \neq 0$, the proposed control law ensures asymptotic stability about the equilibrium ($s_1 = 0$) in the presence of bounded model uncertainty and disturbances.

C. WHEEL SLIP REGULATION

The current study employed a model-based approach for wheel slip regulation motivated by a sliding mode-based controller designed in [31] for HCRVs. To regulate wheel slip at the desired level (λ_{ref}), the sliding surface (s_2) is defined as,

$$s_{2,ij}(t) = \lambda_{ij}(t) - \lambda_{ij,ref}. \tag{37}$$

Here, the value of λ_{ref} is assumed to be known and constant for the given tire-road interface. Subsequently, the derivative of the sliding function yields,

$$\dot{s}_{2,ij}(t) = \dot{\lambda}_{ij}(t). \tag{38}$$

Utilizing PRERL and substituting the derivative of wheel slip from (13), the control input for wheel slip regulation was obtained as,

$$\begin{aligned}\left(\tau_{b,ij}(t)\right)_{wsr} = \frac{1}{g_{ij}(t)}\Bigg[&-f_{ij}\Big(\lambda_{ij}(t), t\Big) \\ &- \frac{K_2|s_{2,ij}(t)|^{\beta_2}\mathrm{sgn}(s_{2,ij}(t))}{\delta_2 + (1-\delta_2)e^{-\gamma_2|s_{2,ij}(t)|^{\phi_2}}}\Bigg],\end{aligned} \tag{39}$$

where K_2, β_2, δ_2, γ_2, and ϕ_2 are controller parameters, and subscript $(\cdot)_{wsr}$ indicates its affiliation to WSR.

D. COORDINATION STRATEGY FOR DYC+WSR

Load is transferred from rear to front axle and inner to outer wheels in combined cornering and braking. Hence, the coordination strategy in the current study involved regulating force on the front inner/outer wheel as per the required external yaw moment from DYC. The rest of the wheels were operated with the WSR algorithm's input to maximize the braking force. This study found that such a single-wheel differential braking strategy was sufficient to produce the required magnitude of external yaw moment for the vehicle's

laden and unladen configurations. It helped track reference yaw rate without a significant increase in braking distance. Thus, a counter-clockwise external yaw moment ($M_{z,\text{ext}} < 0$) was generated by reducing the brake force on the front outer wheel and clockwise ($M_{z,\text{ext}} > 0$) by reducing on the front inner wheel. The desired brake force, for example, at the front outer wheel (front right in case of a left turn) to generate the required external counter-clockwise yaw moment was determined using the total yaw moment of braking forces, expressed as,

$$\left(F_{b,fr}\right)_{\text{dyc}} = \frac{2}{T_f}\Bigg(\left(M_{z,\text{ext}}(t)\right)_{\text{dyc}} + \frac{T_f}{2}\left(F_{b,fl}\right)_{\text{wsr}} + \frac{T_r}{2}\left(F_{b,rl}\right)_{\text{wsr}} - \frac{T_f}{2}\left(F_{b,rr}\right)_{\text{wsr}}\Bigg). \quad (40)$$

The obtained brake force was converted into desired pressure (P_{des}) using the wheel dynamics equation in (8). This desired pressure was provided to the inner-loop brake controller to realize the braking force.

E. BRAKE CONTROLLER

Pneumatic brake actuators are typically sluggish in their transient response and require performance enhancement for effective operation in an AVSS. Also, cascaded control operations with a time-delayed system are known to induce oscillations in its reference input regulation performance [31], [32]. This calls for implementing a brake controller and an appropriate delay compensation technique to improve the brake system's performance. Consequently, a PID controller was incorporated while compensating for the delay using a state predictor expressed as,

$$\begin{aligned} \bar{x}_b(t) &= e^{A_b t}x_b + \int_0^{-T_d} e^{-A_b(T_d+\theta)}B_b u(t+\theta)d\theta, \\ &\quad -T_d \le \theta \le 0, \\ \bar{P}_{\text{act}} &= C_b\bar{x}_b(t), \end{aligned} \quad (41)$$

where $\bar{x}_b$ is the predicted state, and $\bar{P}_{\text{act}}$ is the predicted brake chamber pressure. Its function was to use the current states and previous delay period's inputs to predict the state and output for the subsequent delay period. These were employed in the feedback path of the controller to compare with the desired value and obtain control input (Fig. 3).

IV. HARDWARE-IN-LOOP EXPERIMENTAL RESULTS

The framework was tested using the Hardware-in-Loop setup shown in Fig. 4. The hardware setup consisted of a front and rear axle of a 16-tonne truck equipped with a pneumatic brake system. An EPR regulated the pressure at each brake chamber, and pressure sensors measured the pressure. The brake system hardware was interfaced with the host computer through a real-time hardware platform (IPG Xpack4®). The control algorithm was realized using MATLAB-Simulink® and was converted to C code for exporting to IPG Xpack4®. The virtual vehicle parameters and other test conditions like the road and friction properties were specified from the host

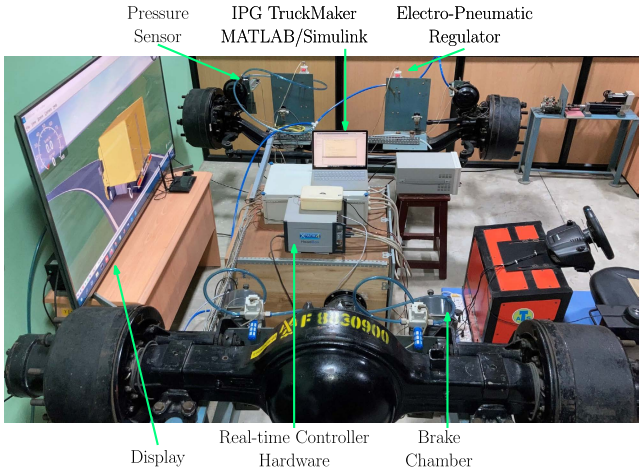

FIGURE 4. Hardware-in-Loop setup for a pneumatic brake system.

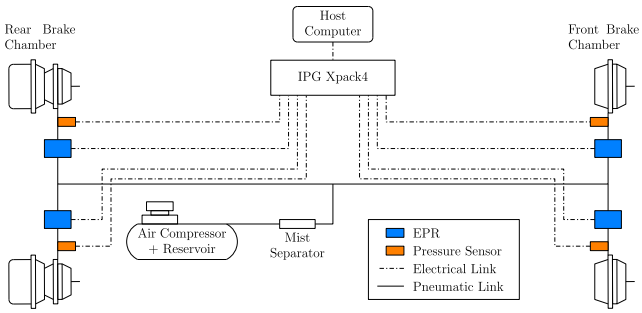

FIGURE 5. Hardware-in-Loop setup schematic representation.

computer in IPG TruckMaker®, a comprehensive vehicle dynamics simulation software package for trucks. The brake system component in the virtual vehicle was replaced with the hardware, thus resulting in hardware-in-loop co-simulation (refer Fig. 5).

The algorithm's performance was evaluated for a 150 m radius (left) J-turn maneuver on a road surface with a peak longitudinal friction coefficient (μ_{px}) of 0.5 (having $\lambda_{\text{ref}} = 10\%$) representative of a wet road surface. A mid-level friction surface was chosen considering the saturation of lateral forces for high slip angles and its impact on directional performance. HiL experiments were performed for two cases of steering inputs. For the first case, a fixed profile for steering wheel angle (δ_{sw}) input was given to the vehicle. For the second case, the IPGDriver® module was activated, which enabled the simulated human driver's control action to the vehicle. The inputs to the module included intended path, vehicle position, speed, acceleration, and steering wheel torque [33]. The vehicle was fully braked at an initial speed of $v_x = 60$ km/h when the vehicle entered the corner. Both the unladen ($M = 4700$ kg) and fully laden ($M = 16200$ kg) configurations were considered in the performance evaluation. The test run was terminated when the vehicle's speed dropped below 5 km/h. An open-loop vehicle response where the algorithms are disabled for the aforementioned maneuver indicated wheel lock and lane departure, thus resulting in instability.

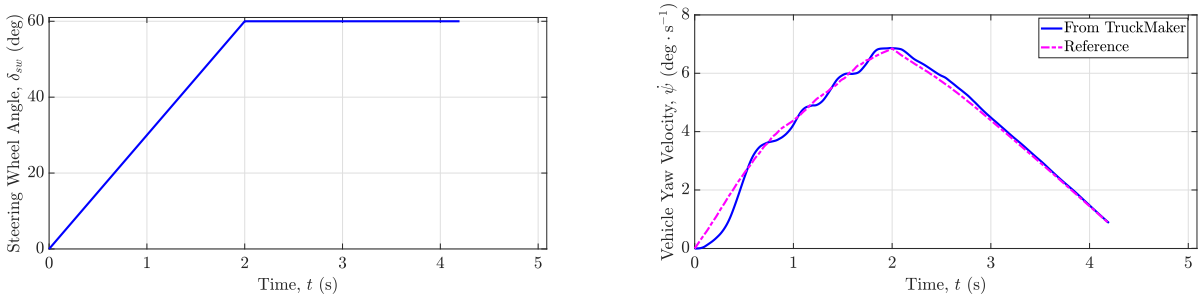

FIGURE 6. DYC$_{(M)}$+WSR$_{(M)}$ algorithm performance for a laden vehicle moving at $v_x = 60$ km/h on a surface whose $\mu_{px} = 0.5$ and radius of curvature is $R_C = 150$ m (Case 1): (a) Steering wheel angle; (b) Yaw rate tracking.

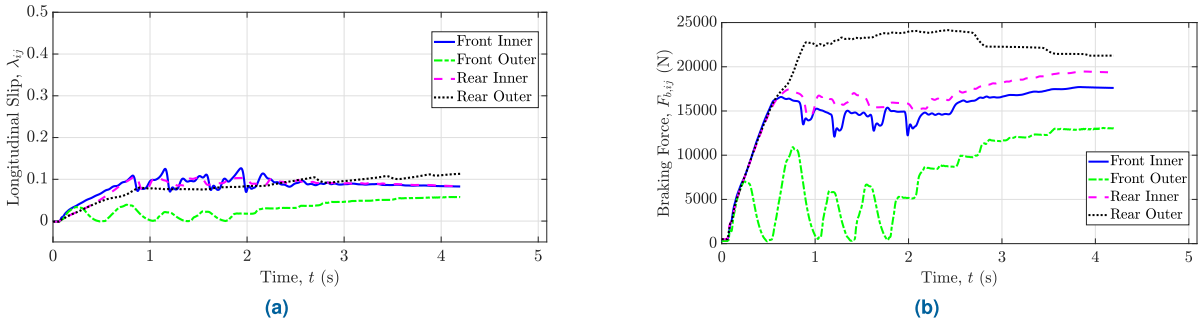

FIGURE 7. DYC$_{(M)}$+WSR$_{(M)}$ algorithm performance for a laden vehicle moving at $v_x = 60$ km/h on a surface whose $\mu_{px} = 0.5$ and radius of curvature is $R_C = 150$ m (Case 1): (a) Longitudinal slip; (b) Brake force.

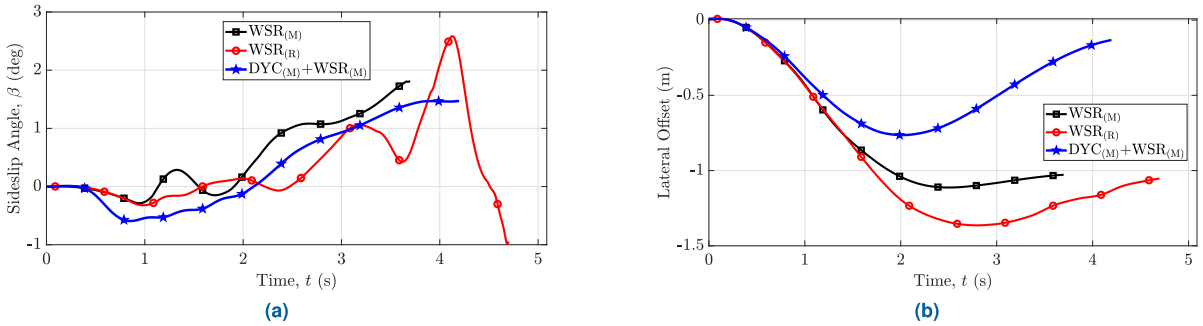

FIGURE 8. Comparison of algorithms for a laden vehicle moving at $v_x = 60$ km/h on a surface whose $\mu_{px} = 0.5$ and radius of curvature is $R_C = 150$ m (Case 1): (a) Vehicle sideslip; (b) Lateral offset.

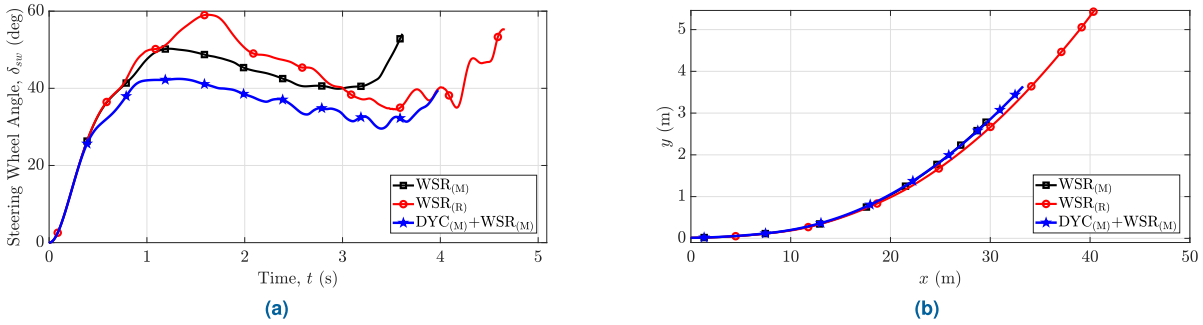

FIGURE 9. Comparison of algorithms for a laden vehicle moving at $v_x = 60$ km/h on a surface whose $\mu_{px} = 0.5$ and radius of curvature is $R_C = 150$ m (Case 2): (a) Steering wheel angle; (b) Vehicle trajectory.

A comparison study of DYC+WSR with standalone model-based and rule-based WSR algorithms was conducted to evaluate the algorithms during combined cornering and emergency braking. As a standalone model-based WSR, the brake torque calculated in Section III-C that regulates the slip at a reference value was applied to all wheels through the brake controller with delay compensation. For rule-based WSR, the 3-phase combined wheel

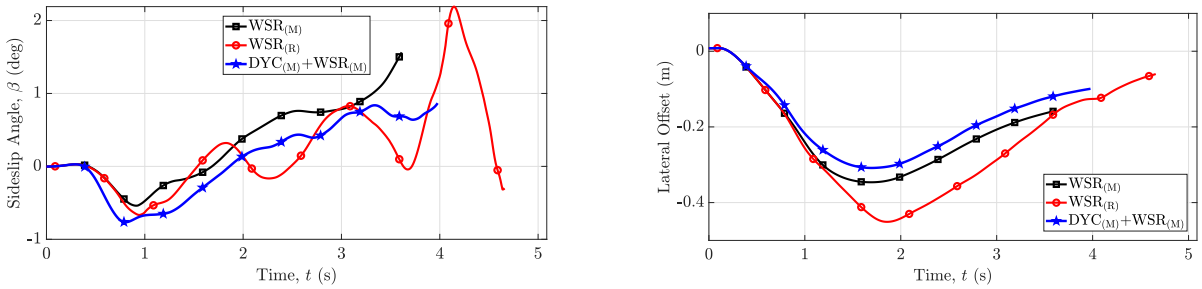

FIGURE 10. Comparison of algorithms for a laden vehicle moving at $v_x = 60$ km/h on a surface whose $\mu_{px} = 0.5$ and radius of curvature is $R_C = 150$ m (Case 2): (a) vehicle sideslip; (b) lateral offset.

slip and acceleration threshold algorithm developed in [34] was considered. The following notation is adopted to distinguish the algorithms: proposed integrated DYC and WSR by $\text{DYC}_{(\text{M})}$+$\text{WSR}_{(\text{M})}$; standalone model-based WSR by $\text{WSR}_{(\text{M})}$, standalone rule-based WSR by $\text{WSR}_{(\text{R})}$. For discussion, this paper presents the result plots for the laden vehicle alone, and similar results were obtained for the unladen case.

Fig. 6-7 present the closed-loop response of the vehicle implemented with the proposed integrated algorithm. Fig. 6a depicts the fixed steering input to the simulations (Case 1). In Fig. 6b, the yaw rate tracking performance is displayed. The yaw rate tracking index (YTI, deg/s) defined by,

$$\text{YTI} = \frac{\int_{T_{\text{start}}}^{T_{\text{end}}} |\dot{\psi}(t) - \dot{\psi}_{\text{ref}}(t)|\, dt}{T_{\text{end}} - T_{\text{start}}}, \tag{42}$$

where T_{start} is the brake application instant and T_{end} is the simulation end time, was found to be 0.173 deg/s and 0.269 deg/s for the laden and unladen vehicles, respectively. In comparison, $\text{WSR}_{(\text{M})}$ and $\text{WSR}_{(\text{R})}$ showed vehicle understeer behavior ($\dot{\psi} < \dot{\psi}_{\text{ref}}$) throughout the maneuver. Fig. 7a plots the wheel slip for all four wheels. The front inner and rear wheels regulated their slip at the desired level of $\lambda_{\text{ref}} = 10\%$, where the maximum braking force is obtained on a wet road surface. The DYC control input governed braking force predominantly at the front outer wheel to generate external yaw moment for tracking reference yaw rate. Fig. 7b shows the control inputs, that is, the braking forces. Thus, the integrated algorithm achieved yaw rate tracking and successfully executed ABS's primary aim by avoiding wheel lock.

For better stability and handling, a low sideslip angle is considered desirable [12], [13]. Fig. 8a compares sideslip angle with the standalone WSR algorithms where it was confined in the range $(-0.5°, 2°)$ for $\text{DYC}_{(\text{M})}$+$\text{WSR}_{(\text{M})}$ and $\text{WSR}_{(\text{M})}$, while it exceeded up to 2.7° in the case of $\text{WSR}_{(\text{R})}$. Fig. 8b shows the controller's performance in minimizing the deviation of the vehicle from the intended path. The maximum lateral offset of the virtual road sensor (located in the middle of the front axle) projected on the road center-line was obtained as ≈ 0.78 m for $\text{DYC}_{(\text{M})}$+$\text{WSR}_{(\text{M})}$ and was the least among the three algorithms. Thus the integrated algorithm indicated a superior ability to execute cornering with simultaneous braking.

The comparisons with IPGDriver® in the loop (Case 2) are presented in Fig. 9-10. The maximum steering input from the IPGDriver® reached a peak of 42.4° for $\text{DYC}_{(\text{M})}$+$\text{WSR}_{(\text{M})}$, as shown in Fig. 9a. In comparison, $\text{WSR}_{(\text{M})}$ and $\text{WSR}_{(\text{R})}$ showed higher correction from the driver, reaching a peak of 54.1° and 60°, respectively. Consequently, the vehicle closely followed the intended vehicle trajectory, as shown in Fig. 9b, however, at the expense of higher steering effort. The sideslip angle in Fig. 10a was limited to 0.9° with $\text{DYC}_{(\text{M})}$+$\text{WSR}_{(\text{M})}$, whereas, with $\text{WSR}_{(\text{M})}$ and $\text{WSR}_{(\text{R})}$, the peak reached 1.6° and 2°, respectively. As shown in Fig. 10b, the lateral offset was minimized further than Case 1 with aid from IPGDriver® through steering corrections.

A performance index was calculated for each case, considering quantities associated with the lateral dynamics of the vehicle. The index for Case 1 included lateral offset and sideslip angle since the steering input was the same for all three algorithms. The average normalized percentage improvement compared to the open-loop response was evaluated given by the expression,

$$\text{Index}, \% = \frac{1}{2}\left(\frac{(\beta_{m,\text{ol}} - \beta_{m,\text{cl}})}{\beta_{m,\text{ol}}} + \frac{(\Delta_{\text{ol}} - \Delta_{\text{cl}})}{\Delta_{\text{ol}}}\right) \times 100, \tag{43}$$

where β_m is the absolute maximum value of sideslip angle, Δ is the absolute maximum value of lateral offset from the desired trajectory, and subscripts 'ol' and 'cl' respectively stands for open-loop and closed-loop. Similarly, for Case 2, the index included maximum steering input in addition to previously considered parameters. The index accordingly computed is given by,

$$\text{Index}, \% = \frac{1}{3}\left(\frac{(\delta_{m,\text{ol}} - \delta_{m,\text{cl}})}{\delta_{m,\text{ol}}} + \frac{(\beta_{m,\text{ol}} - \beta_{m,\text{cl}})}{\beta_{m,\text{ol}}} + \frac{(\Delta_{\text{ol}} - \Delta_{\text{cl}})}{\Delta_{\text{ol}}}\right) \times 100, \tag{44}$$

where δ_m is the absolute maximum value of steering wheel angle. Table 3 consolidates the evaluated test cases. A few additional severe cases (radius = 100 m) were also considered with the IPGDriver® in loop. The $\text{DYC}_{(\text{M})}$+$\text{WSR}_{(\text{M})}$ algorithm resulted in a minimum 29% improvement over the

TABLE 3. Performance comparison of various algorithms in a combined cornering and emergency braking maneuvers.

S.R. No.	Mass, kg	μ_{px}	Speed, km/h	Radius, m	Algorithm	Performance Parameters: Braking Distance, m	Max. Steering Input, (°)	Max. Sideslip Angle, (°)	Max. Lateral Offset, m	Electrical Energy Consumption[$], mJ	Index, (%)
Case 1: IPGDriver® inactive											
1	16200	0.5	60	150	$WSR_{(M)}$	36.07	60.0	1.8	1.11	151.9	12.7*
2	16200	0.5	60	150	$WSR_{(R)}$	46.69	60.0	2.6	1.36	165.2	-24.6# *
3	16200	0.5	60	150	$DYC_{(M)}$+$WSR_{(M)}$	41.16	60.0	1.5	0.76	131.2	**29.3**
4	4700	0.5	60	150	$WSR_{(M)}$	32.51	45.0	1.5	1.33	18.4	44.2*
5	4700	0.5	60	150	$WSR_{(R)}$	44.24	45.0	2.2	1.68	67.6	15.7*
6	4700	0.5	60	150	$DYC_{(M)}$+$WSR_{(M)}$	37.32	45.0	1.5	0.80	18.9	**41.7**
Case 2: IPGDriver® active											
1	16200	0.5	60	150	$WSR_{(M)}$	34.93	54.1	1.6	0.35	142.1	62.3
2	16200	0.5	60	150	$WSR_{(R)}$	46.10	59.1	2.2	0.45	149.1	49.6
3	16200	0.5	60	150	$DYC_{(M)}$+$WSR_{(M)}$	38.70	42.4	0.9	0.31	135.1	**77.1**
4	4700	0.5	60	150	$WSR_{(M)}$	31.13	48.4	1.1	0.22	19.1	78.6
5	4700	0.5	60	150	$WSR_{(R)}$	43.49	47.6	1.1	0.24	60.8	78.6
6	4700	0.5	60	150	$DYC_{(M)}$+$WSR_{(M)}$	34.45	38.4	0.8	0.18	19.0	**84.1**
Additional test cases: IPGDriver® active											
1	16200	0.5	60	100	$WSR_{(M)}$	35.12	84.3	2.3	0.59	139.3	28.5
2	16200	0.5	60	100	$WSR_{(R)}$	45.77	95.4	2.0	0.72	165.7	34.1
3	16200	0.5	60	100	$DYC_{(M)}$+$WSR_{(M)}$	41.34	68.0	1.1	0.53	143.8	**62.5**
4	4700	0.5	60	100	$WSR_{(M)}$	30.89	75.7	1.9	0.36	18.1	65.3
5	4700	0.5	60	100	$WSR_{(R)}$	44.39	76.8	1.6	0.3	43.9	67.9
6	4700	0.5	60	100	$DYC_{(M)}$+$WSR_{(M)}$	34.97	60.8	1.1	0.18	21.0	**76.8**

[$] The electrical energy consumption by the EPRs is indicative of the air consumption.

[#] The index is negative due to excess sideslip angle compared to the open-loop case.

[*] The vehicle was found to leave a 3.5 m wide road.

open-loop response in all cases while tracking yaw rate and ensuring vehicle directional stability. It also improved the performance in the range of 5% to 53% over standalone WSR in various emergency test cases.

Overall, the braking distance was least for $WSR_{(M)}$ and highest for $WSR_{(R)}$. Higher braking distance in the rule-based algorithm was attributed to pump-hold-exhaust phases of brake pressure, which resulted in wheel slip cycling in a band around the reference value [34]. These characteristics also resulted in momentary wheel locks during combined cornering and emergency braking (permitted in ABS operation) that impacted the directional response of the vehicle (manifested in high sideslip angle and understeer behavior). On the other hand, standalone model-based WSR regulated wheel slip around the peak value to generate maximum braking forces at all four wheels; however, it compromised lateral force generation and thus the directional performance of the vehicle.

The $DYC_{(M)}$+$WSR_{(M)}$ governed the front inner/outer wheel's braking force to regain the lateral force and track the reference yaw rate. The sideslip angle response was stable in all the cases and had a lower absolute peak value than the other two algorithms. Thus, the directional stability was enhanced by the $DYC_{(M)}$+$WSR_{(M)}$, however, at some expense of braking distance. Therefore, the proposed 'integrated direct yaw-moment and wheel slip regulation' algorithm set a benchmark for an effective trade-off between the directional performance and braking distance.

V. CONCLUSION

Combined cornering and emergency braking scenarios requiring ABS intervention were analyzed through HiL experiments. A framework for integrated DYC and WSR was presented to ensure vehicle directional stability and performance. In summary, the following are the contributions of this study:

- A direct yaw-moment controller was designed using a robust sliding mode controller and including roll dynamics.
- A modified model-based wheel slip regulation algorithm was presented that perform effectively in combined cornering and braking scenario.
- The brake force allocation strategy based on single wheel control for generating the desired external yaw moment was shown to work in all severe maneuvers tested for the vehicle.
- The study established that the standalone WSR algorithm retained the vehicle stability; however, it did not perform satisfactorily in directional stability and performance. Moreover, the momentary wheel lock permitted in ABS operation can lead to excess sideslip angle.
- Yaw rate control in coordination with an efficient wheel slip regulation algorithm was demonstrated to achieve directional stability while keeping the sideslip in check.
- The quantitative evaluation also suggested the enhancement in lateral performance by incorporating the

integrated DYC and WSR compared to standalone ABS operation.

APPENDIX A
DEFINITIONS

The definitions of coefficients in (24) are as follows:

$$\begin{aligned}
\Theta_1 &= -2\left(C_{\alpha f} + C_{\alpha r}\right),\\
\Theta_2 &= -Mv_x - \frac{2\left(C_{\alpha f}L_f - C_{\alpha r}L_r\right)}{v_x},\\
\Theta_3 &= 2\left(C_{\alpha f}C_{\epsilon f} + C_{\alpha r}C_{\epsilon r}\right),\\
\Theta_4 &= -2\left(C_{\alpha f}L_f - C_{\alpha r}L_r\right),\\
\Theta_5 &= -\frac{2\left(C_{\alpha f}L_f^2 + C_{\alpha r}L_r^2\right)}{v_x},\\
\Theta_6 &= 2\left(C_{\alpha f}L_f C_{\epsilon f} - C_{\alpha r}L_r C_{\epsilon r}\right).
\end{aligned}$$

The definitions of coefficients in (29) are as follows:

$$\begin{aligned}
B_\beta &= -\frac{2M_s h_s I_{xz}}{D}\left(C_{\alpha f} + C_{\alpha r}\right)\\
&\quad -\frac{2(M_s^2 h_s^2 - MI_x)}{D}\left(C_{\alpha f}L_f - C_{\alpha r}L_r\right),\\
B_r &= -\frac{M_s h_s I_{xz}}{D}\left(Mv_x(t) + \frac{2\left(C_{\alpha f}L_f - C_{\alpha r}L_r\right)}{v_x(t)}\right)\\
&\quad -\frac{2(M_s^2 h_s^2 - MI_x)}{Dv_x(t)}\left(C_{\alpha f}L_f^2 + C_{\alpha r}L_r^2\right)\\
&\quad +\frac{MM_s h_s I_{zx} v_x(t)}{D},\\
B_\phi &= \frac{2M_s h_s I_{xz}}{D}\left(C_{\alpha f}C_{\epsilon f} + C_{\alpha r}C_{\epsilon r}\right)\\
&\quad +\frac{2(M_s^2 h_s^2 - MI_x)}{D}\left(C_{\alpha f}L_f C_{\epsilon f} - C_{\alpha r}L_r C_{\epsilon r}D\right)\\
&\quad +\frac{MI_{xz}(M_s g h_s - K_\phi)}{D},\\
B_p &= -\frac{MI_{xz}C_\phi}{D},\\
B_\delta &= \frac{2M_s h_s I_{xz}C_{\alpha f}}{D} + \frac{2(M_s^2 h_s^2 - MI_x)C_{\alpha f}L_f}{D},\\
B_\tau &= \frac{(M_s^2 h_s^2 - MI_x)}{D},\\
D &= M_s^2 h_s^2 I_z + MI_{zx}^2 - MI_z I_x.
\end{aligned}$$

REFERENCES

[1] *Global Status Report on Road Safety 2018*, World Health Organization, Geneva, Switzerland, 2018.
[2] Ministry of Road Transport & Highways. (2020). *Road Accidents in India 2019*. [Online]. Available: http://www.morth.nic.in
[3] Federal Register. (2012). *Electronic Stability Control Systems for Heavy Vehicles*. [Online]. Available: https://www.federalregister.gov
[4] Ministry of Road Transportation and Highways. (2014). *Central Motor Vehicles (9th Amendment) Rules, 2014*. [Online]. Available: http://egazette.nic.in/
[5] M. Abe, "Side-slip control to stabilize vehicle lateral motion by direct yaw moment," *JSAE Rev.*, vol. 22, no. 4, pp. 413–419, Oct. 2001.
[6] M. Mirzaei, "A new strategy for minimum usage of external yaw moment in vehicle dynamic control system," *Transp. Res. C, Emerg. Technol.*, vol. 18, no. 2, pp. 213–224, Apr. 2010.
[7] M. Choi and S. B. Choi, "Model predictive control for vehicle yaw stability with practical concerns," *IEEE Trans. Veh. Technol.*, vol. 63, no. 8, pp. 3539–3548, Oct. 2014.
[8] C. Feng, N. Ding, and Y. He, "An integrated control algorithm of ABS and DYC for emergency braking on a μ-split road," in *Proc. Int. Conf. Control Eng. Commun. Technol.*, Dec. 2012, pp. 516–522.
[9] H. Mirzaeinejad and M. Mirzaei, "Optimization of nonlinear control strategy for anti-lock braking system with improvement of vehicle directional stability on split-μ roads," *Transp. Res. C, Emerg. Technol.*, vol. 46, pp. 1–15, Sep. 2014.
[10] M. S. Bang, S. H. Lee, C. S. Han, D. B. Maciuca, and J. K. Hedrick, "Performance enhancement of a sliding mode wheel slip controller by the yaw moment control," *Proc. Inst. Mech. Eng. D, J. Automobile Eng.*, vol. 215, no. 4, pp. 455–468, Apr. 2001.
[11] K. Yi, T. Chung, J. Kim, and S. Yi, "An investigation into differential braking strategies for vehicle stability control," *Proc. Inst. Mech. Eng. D, J. Automobile Eng.*, vol. 217, no. 12, pp. 1081–1093, 2003.
[12] G. Morrison and D. Cebon, "Combined emergency braking and turning of articulated heavy vehicles," *Vehicle Syst. Dyn.*, vol. 55, no. 5, pp. 725–749, May 2017.
[13] Z. Wang, J. Zhu, L. Zhang, and Y. Wang, "Automotive ABS/DYC coordinated control under complex driving conditions," *IEEE Access*, vol. 6, pp. 32769–32779, 2018.
[14] S. Li, J. Zhao, S. Yang, and H. Fan, "Research on a coordinated cornering brake control of three-axle heavy vehicles based on hardware-in-loop test," *IET Intell. Transp. Syst.*, vol. 13, no. 5, pp. 905–914, May 2019.
[15] J. Slotine and W. Li, *Applied Nonlinear Control*. Upper Saddle River, NJ, USA: Prentice-Hall, 1991.
[16] K. B. Devika and S. Thomas, "Power rate exponential reaching law for enhanced performance of sliding mode control," *Int. J. Control Automat. Syst.*, vol. 15, no. 6, pp. 2636–2645, Dec. 2017.
[17] R. Rajamani, *Vehicle Dynamics and Control*. Berlin, Germany: Springer, 2011.
[18] R. Limpert, *Brake Design and Safety*. Warrendale, PA, USA: Society of Automotive Engineers, 1999.
[19] A. S. Trigell, M. Rothhämel, J. Pauwelussen, and K. Kural, "Advanced vehicle dynamics of heavy trucks with the perspective of road safety," *Vehicle Syst. Dyn.*, vol. 55, no. 10, pp. 1572–1617, Oct. 2017.
[20] M. Abe, *Vehicle Handling Dynamics: Theory and Application*. Oxford, U.K.: Butterworth-Heinemann, 2015.
[21] U. Kiencke and L. Nielsen, *Automotive Control Systems*. Berlin, Germany: Springer, 2005.
[22] H. Pacejka, *Tyre and Vehicle Dynamics*. Oxford, U.K.: Butterworth-Heinemann, 2012.
[23] *Reference Manual Version 8.0 TruckMaker*, IPG Automotive, Karlsruhe, Germany, 2019.
[24] N. Sridhar, K. V. Subramaniyam, S. C. Subramanian, G. Vivekanandan, and S. Sivaram, "Model based control of heavy road vehicle brakes for active safety applications," in *Proc. 14th IEEE India Council Int. Conf. (INDICON)*, Dec. 2017, pp. 1–6.
[25] S. Khaleghian, A. Emami, and S. Taheri, "A technical survey on tire-road friction estimation," *Friction*, vol. 5, no. 2, pp. 123–146, Jun. 2017.
[26] M. Viehweger, C. Vaseur, S. van Aalst, M. Acosta, E. Regolin, A. Alatorre, W. Desmet, F. Naets, V. Ivanov, A. Ferrara, and A. Victorino, "Vehicle state and tyre force estimation: Demonstrations and guidelines," *Vehicle Syst. Dyn.*, vol. 59, no. 5, pp. 675–702, May 2021.
[27] T. A. Wenzel, K. J. Burnham, M. V. Blundell, and R. A. Williams, "Dual extended Kalman filter for vehicle state and parameter estimation," *Vehicle Syst. Dyn.*, vol. 44, no. 2, pp. 153–171, 2006.
[28] G. Morrison and D. Cebon, "Sideslip estimation for articulated heavy vehicles at the limits of adhesion," *Vehicle Syst. Dyn.*, vol. 54, no. 11, pp. 1601–1628, 2016.
[29] N. Ahmadian, A. Khosravi, and P. Sarhadi, "Driver assistant yaw stability control via integration of AFS and DYC," *Vehicle Syst. Dyn.*, vol. 60, no. 5, pp. 1742–1762, May 2022.
[30] X. Jin, J. Wang, Z. Yan, L. Xu, G. Yin, and N. Chen, "Robust vibration control for active suspension system of in-wheel-motor-driven electric vehicle via μ-synthesis methodology," *J. Dyn. Syst., Meas., Control*, vol. 144, no. 5, May 2022, Art. no. 051007.
[31] N. Sridhar, K. B. Devika, S. C. Subramanian, G. Vivekanandan, and S. Sivaram, "Antilock brake algorithm for heavy commercial road vehicles with delay compensation and chattering mitigation," *Vehicle Syst. Dyn.*, vol. 59, no. 4, pp. 526–546, Apr. 2021.

[32] K. Devika, N. Sridhar, H. Patil, and S. C. Subramanian, "Delay compensated pneumatic brake controller for heavy road vehicle active safety systems," *Proc. Inst. Mech. Eng. C, J. Mech. Eng. Sci.*, vol. 235, no. 13, pp. 2333–2346, Jul. 2021.
[33] *User Manual Version 8.1 IPGDriver*, IPG Automotive, Karlsruhe, Germany, 2019.
[34] A. Challa, K. Ramakrushnan, P. V. Gaurkar, S. C. Subramanian, G. Vivekanandan, and S. Sivaram, "A 3-phase combined wheel slip and acceleration threshold algorithm for anti-lock braking in heavy commercial road vehicles," *Vehicle Syst. Dyn.*, pp. 1–22, Mar. 2021, doi: 10.1080/00423114.2021.1903048.

HARSHAL PATIL received the B.Tech. degree in mechanical engineering from the Vishwakarma Institute of Technology, Pune, in 2015. He is currently pursuing the Ph.D. degree in vehicle dynamics and controls with the Department of Engineering Design, Indian Institute of Technology (IIT) Madras, Chennai, India. His research interests include control of automotive systems and design of active vehicle safety systems.

K. B. DEVIKA (Member, IEEE) received the Ph.D. degree in control systems from the National Institute of Technology Calicut, India. She was a Postdoctoral Fellow with the Department of Engineering Design, IIT Madras, India, when the research presented in this study was carried out. Currently, she is a Lecturer in mechanical engineering with the University of Exeter, U.K. Her research interests include safe automobiles and clean transportation systems.

GUNASEKARAN VIVEKANANDAN received the B.Tech. degree in automobile engineering from the Madras Institute of Technology, Anna University, Chennai, India. He has worked in various auto component and OE industries for the past 28 years. He is currently working as the Sr. General Manager of research and development with Madras Engineering Industries Private Ltd., Chennai, engaged in the business of automotive brake and clutch products.

SRIRAM SIVARAM received the B.Tech. degree in civil engineering from the Indian Institute of Technology Madras, India, and the M.S. and M.B.A. degrees from Cornell University, USA. He is currently the President of Madras Engineering Industries Private Ltd., an automotive component manufacturer based in Chennai, India. Over the past 25 years, he has been directly involved in the development of a variety of new technologies and products and commercializing them.

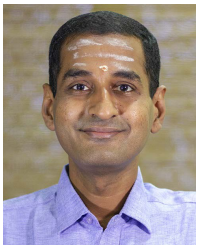

SHANKAR C. SUBRAMANIAN (Senior Member, IEEE) received the B.E. degree in mechanical engineering from the Motilal Nehru Regional Engineering College, India, and the M.S. and Ph.D. degrees from Texas A&M University, USA. He is currently a Professor and a V. Ramamurti Faculty Fellow with the Department of Engineering Design, Indian Institute of Technology (IIT) Madras, Chennai, India. His research interests include dynamics and control with applications to automotive and transportation systems.